Journal of Applied Mechanics and Technical Physics, Vol. 36, No. 2, 1995

TURBULENT SWIRLING WAKE BEHIND A SPHERE WITH COMPLETE OR PARTIAL DRAG COMPENSATION

V. A. Kostomakha and N. V. Lesnova

UDC 537.517.4

An experimental study has been made of the axisymmetric turbulent wake behind a sphere, which was immersed in a uniform airstream and whose hydrodynamic drag was completely or partially balanced by the momentum of a jet injected into the back of the sphere. The formulation of the problem and the form of the model are the same as those used in [1]. The principal difference from previous experiments is that the jet was swirling. It has been demonstrated that even a weak swirling of the stream by the propeller causes a momentumless wake to develop behind the sphere. As a result the turbulence characteristics degenerate more slowly and the transverse dimensions of the wake grow.

1. The longitudinal component of the excess momentum J and the angular momentum M are important integrated characteristics of the hydrodynamic wake behind the body. Nonswirling wakes behind towed bodies have been studied in greatest detail. In such wakes $J = F_x$ and $M = 0$, where F_x is the drag of the body.

Wakes behind bodies with a propeller have been studied less. If the propeller does not cause swirls in the stream, then as before $M = 0$ in the wake. In uniform rectilinear motion the drag of the body is completely balanced by the propulsion of the propeller thrust and $J = 0$ in the wake behind the body. Such a momentumless wake was studied experimentally [1-7] and theoretically or numerically [8-15]. The laws of development of hydrodynamic wakes after self-propelled and towed bodies were found to differ greatly.

The influence that swirling of the stream has on the dynamics of a momentumless wake was studied in experiments [3, 4]. Shetz and Jakubowski [3] studied two methods of producing self-propulsion: the drag of an appropriately streamlined thin body of rotation was balanced by an annular jet, which did not cause swirling, and a propeller mounted at the rear of the body. In their conclusions they pointed out that the rate of degeneration of the axial velocity component is the same for both cases of self-propulsion considered, starting from a small distance from the body and swirling has almost no effect on the mean velocity field. Similar conclusions were obtained in [4], where a momentumless wake was also produced with a well streamlined body with a "jet engine," whose jet swirled in one series of experiments and did not in another series.

Analysis in [16-19] of the asymptotic behavior of perturbations of the mean velocity in a self-similar swirling wake, however, showed that the existence of a tangential velocity component, even a small one, appreciably affects the flow pattern in the wake and this influence is traced at rather large distances from the body. The experimental data reported below illustrate how swirling of the stream affects the evolution of the momentumless wake behind a sphere and also give an idea of the distinctive features of wake development, depending on the ratio of J and M.

2. The experiments were carried out in a low-turbulence wind tunnel with a closed throat 4 m long and 0.4 x 0.4 m in cross section. A sphere of diameter $D = 25$ mm, mounted on a tube with an outside diameter of 8 mm, was fastened on anchor wires made of tungsten filament 0.1 mm in diameter at the beginning of the throat, as shown in Fig. 1*a*, where *1* is the sphere, *2* is the tube which delivered air, *3* are anchor wires, and *4* is the throat of the wind tunnel. A special nozzle with an inside diameter of 6 mm was built into the sphere to form a swirling jet that flowed from the rear of the sphere. The stream was caused to swirl by the tangential admission of air through three rows of 1-mm holes In order to ensure moderate swirling (without return currents forming in the neighborhood of the outlet section of the internal channel) and sufficient thrust, the bottom of the nozzle had an extra hole, whose diameter was chosen experimentally.

Figure 1 shows the Cartesian coordinate system used in the measurements, with origin at the back of the sphere, and a cylindrical coordinate system bound to it, in which the results are shown.

M. A. Lavrent'ev Institute of Hydrodynamics, Siberian Division of the Russian Academy of Sciences, 630090 Novosibirsk. Translated from Prikladnaya Mekhanika i Tekhnicheskaya Fizika, No. 2, pp. 88-98, March-April, 1995. Original article submitted April 27, 1994; revision submitted June 1, 1994.

 0021-8944/95/3602-0226$12.50

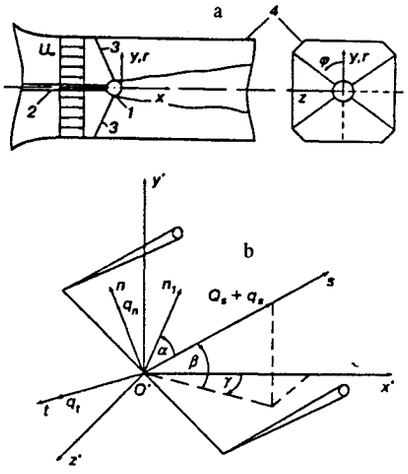

Fig. 1

In order to set the model at zero angle of attack to the mainstream and to determine the position of the axis of the wake the dispersion of the longitudinal component of the velocity fluctuations was measured in two mutually perpendicular directions in the planes $\varphi = 0$ and $\varphi = \pi/2$, which are indicated by dashed lines in Fig. 1.

The velocity was measured by hot-wire anemometric equipment made by DISA (55D05 hot-wire anemometer and 55D15 linearizer). The sensing element of the sensor of the hot-wire anemometer was made of gold-plated or platinum-plated tungsten filament with a diameter of 5 μm and a length of 1.25 mm or 1.5 mm for a single-filament or double-filament sensor, respectively.

In the experiments we measured three velocity components, i.e., longitudinal U, radial V, and tangential W, as well as six components of the Reynolds stress tensor $\langle u^2\rangle$, $\langle v^2\rangle$, $\langle w^2\rangle$, $\langle uv\rangle$, $\langle uw\rangle$, $\langle vw\rangle$, where u, v, and w are the longitudinal, radial, and tangential components of the velocity fluctuations and the angular brackets denote averaging.

Information about these quantities by means of hot-wire anemometers can be obtained in at least two ways:

1. Measurements are made for six different positions of the sensor filament relative to the chosen coordinate system. Such positions are obtained, e.g., by continuously rotating the sensor about its axis [20] or by successively setting the sensor in several fixed positions in space [21]. The unknown quantities are determined from the solution of a nonlinear system of algebraic equations, using an iteration procedure. This method is evidently the only one that is acceptable for measuring the characteristics of turbulence in flows bounded by hard walls, e.g., in a swirling turbulent flow in a round pipe.

2. A single-filament inclined sensor or, preferably, a double-filament sensor with twisted filaments, is oriented in the stream so that the axis of the sensor is in the direction of the mean velocity vector. An example of such orientation of one filament of a double-filament sensor is illustrated in Fig. 1*b*. Here $x'y'z'$ is an auxiliary rectangular coordinate system, which is bound to the point of measurements. Its axis is parallel to the axes of the xyz coordinate system. Since the measurements were made in fixed sections only along the z and y axes, the direction of the velocity vector at a given point was determined by measuring two angles: the angle β between the velocity vector and its projection onto the $x'-z'$ plane and the angle γ between that projection and the x' axis. The necessary manipulations of the sensor were made with a special coordinate device, which keeps the axis of the sensing element at a given point as the sensor rotates about the z' and y' axes and about its own axis. The angles of rotation were measured with slide wires.

The procedure for determining the turbulence characteristics for a sensor when the direction of its axis coinciding with the mean velocity vector does not require a system of algebraic solutions to be solved and is almost the same as the method of measurement in a flow that is turbulent on average [22]. If the plane of the sensor coincides with the *s-n* plane (Fig. 1*b*, where $O'n$ is the normal to $O's$, $O't$ is the normal to the plane of the sensor, n_1 is the normal in the plane of the sensor to the filament, α is the angle between that normal and the direction of the mean velocity vector, Q_s and q_s, and q_n and q_t are the average and pulsation components of the velocity vector, respectively, in the *snt* system), then the measured average output signal from the hot-wire anemometer, and the variance of the sum, the difference, and the difference of the variances of the fluctuation components from each of the filaments give information about Q_s, $\langle q^2_n\rangle$, $\langle q^2_s\rangle$, and $\langle q_s q_n\rangle$. Similar measurements

TABLE 1

No. of regime	J'	M'	s	s_1	β_x
1	-0,0126	0,0044	-0,70	0,34	-0,37
2	-0,0047	0,0058	-2,47	0,56	-0,14
3	0,0	0,0070	∞	1,10	0,0
4	0,0028	0,0076	5,43	1,54	0,08
5	0,0053	0,0079	2,98	2,11	0,15

in the s-t plane make it possible to find $\langle q_t^2 \rangle$ and $\langle q_s\, q_t \rangle$. To measure the inadequate correlation of $\langle q_n\, q_t \rangle$, the sensor, which has previously been oriented along the mean velocity vector, is turned about its axis by $\pm$ 45°.

The formulas for converting the parameters of the output signal of the hot-wire anemometer to the turbulence characteristic (see [22]) contain the geometric angle α, whose tangent is determined by the ratio of the sensitivity of a sensor with infinitely long ideal straight filaments to different components of the velocity fluctuations. For actual sensors, however, the directional sensitivity depends on the asymmetry of the temperature distribution along the filament, which is due to the finite length of the filament, how the filament is attached, the aerodynamics of the flow past it, possible deformation as a result of heating and aerodynamic actions, etc. Since the above factors cannot yet be taken into account in advance, a number of experimenters [23, 24] believe that the most reliable method is to calibrate the sensor along the direction in order to determine an "effective" angle α_e.

Calculations done by the method proposed in [23] showed that α_e may differ from the angle $\alpha = \pm$ 45° by roughly $\pm$ 7°. To estimate the possible error due to the usual replacement of α_e by α, it is sufficient to consider the following example: $\tan \alpha_e$ varies from 1.0 for $\alpha_e = \pm$ 45° to 1.1 for $\alpha_e = \pm$ 48°. Comparison of the more complex method of determining α_e with that used here showed that the latter gives entirely satisfactory results.

The turbulence characteristics measured in the snt coordinate system are then converted to the $xr\varphi$ system for known angles α and β on a computer by the following formulas:

components of the mean velocity

$$U = Q_s \cos\beta \cos\gamma, \quad V = Q_s \sin\beta, \quad W = Q_s \cos\beta \sin\gamma,$$

normal Reynolds stresses

$$\begin{aligned}
\langle u^2 \rangle &= \langle q_s^2 \rangle \cos^2\beta \cos^2\gamma + \langle q_n^2 \rangle \cos^2\gamma \sin^2\beta + \langle q_t^2 \rangle \sin^2\gamma - \\
&\quad - \langle q_s q_n \rangle \sin 2\beta \cos^2\gamma - \langle q_s q_t \rangle \sin 2\gamma \cos\beta - \langle q_n q_t \rangle \sin 2\gamma \sin\beta, \\
\langle v^2 \rangle &= \langle q_s^2 \rangle \sin^2\beta + \langle q_n^2 \rangle \cos^2\beta + \langle q_s q_n \rangle \sin 2\beta, \\
\langle w^2 \rangle &= \langle q_s^2 \rangle \cos^2\beta \sin^2\gamma + \langle q_n^2 \rangle \sin^2\beta \sin^2\gamma + \langle q_t^2 \rangle \cos^2\gamma - \\
&\quad - \langle q_s q_n \rangle \sin^2\gamma \sin^2\beta + \langle q_s q_t \rangle \cos\beta \sin 2\gamma - \langle q_n q_t \rangle \sin\beta \sin 2\gamma,
\end{aligned}$$

tangential Reynolds stresses

$$\begin{aligned}
\langle uv \rangle &= (\langle q_s^2 \rangle - \langle q_n^2 \rangle) \cos\gamma \sin 2\beta/2 + \langle q_s q_n \rangle \cos\gamma \cos 2\beta - \\
&\quad - \langle q_s q_t \rangle \sin\gamma \sin\beta - \langle q_n q_t \rangle \sin\gamma \cos\beta, \\
\langle uw \rangle &= (\langle q_s^2 \rangle \cos^2\beta + \langle q_n^2 \rangle \sin^2\beta - \langle q_t^2 \rangle) \sin 2\gamma/2 - \langle q_s q_n \rangle \sin 2\gamma \sin 2\beta/2 + \\
&\quad + \langle q_s q_t \rangle \cos\beta \cos 2\gamma - \langle q_n q_t \rangle \cos 2\gamma \sin\beta, \\
\langle vw \rangle &= (\langle q_s^2 - q_n^2 \rangle) \sin\gamma \sin 2\beta/2 + \langle q_s q_n \rangle \sin\gamma \cos 2\beta + \\
&\quad + \langle q_s q_t \rangle \sin\beta \cos\gamma + \langle q_n q_t \rangle \cos\beta \cos\gamma.
\end{aligned}$$

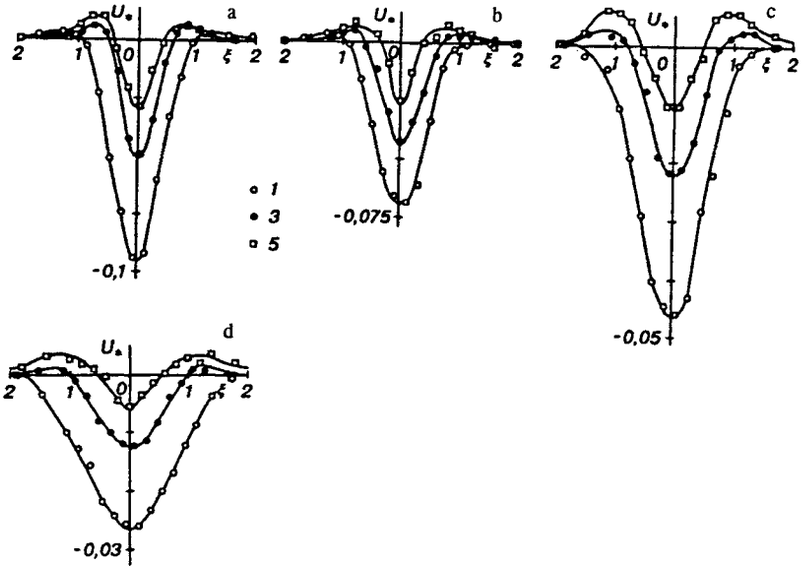

Fig. 2

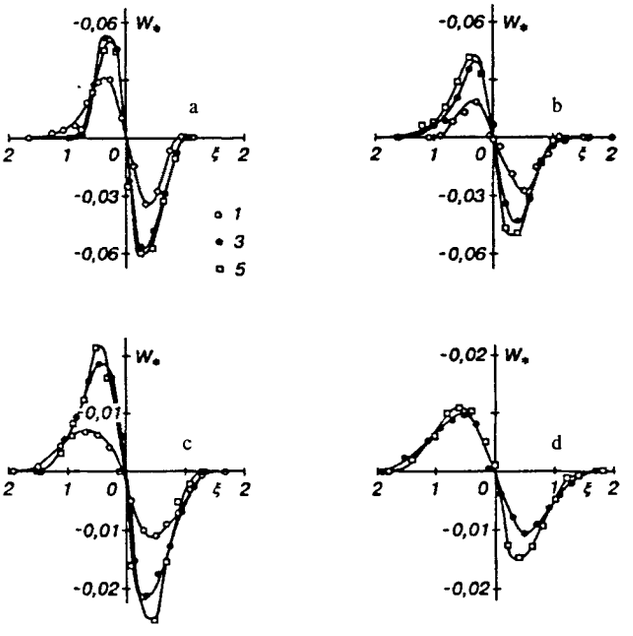

Fig. 3

Customarily, the relative influence of the excess momentum and the angular momentum in free turbulent swirling flows is characterized by the swirl parameter $s = 2M/JD_c$, where D_c is the diameter of the nozzle from which the jet emerges, and J and M are calculated from

$$J = 2\pi\rho \int_0^\infty [U_\infty U_1 - W^2/2 + \langle u^2 \rangle - (\langle v^2 \rangle + \langle w^2 \rangle)/2]\, r\, dr; \tag{2.1}$$

$$M = 2\pi\rho \int_0^\infty (U_\infty W + \langle uw \rangle) r^2\, dr. \tag{2.2}$$

Here U_∞ is the velocity of the mainstream, $U_1 = U - U_\infty$ is the deficit of the longitudinal component of the mean velocity, and ρ is the density of the liquid.

The degree of swirl so determined is constant for the given conditions of jet efflux and the flow around the body and does not depend on the relative elongation $\zeta = x/D$. As $J \to 0$ ($J = 0$ corresponds to a momentumless wake), however, $s \to \infty$ although the swirl may be small. For wakes with nearly zero J, therefore, it is preferred to use a different definition of the measure of swirl. As such a measure it is convenient to take the ratio of the maximum value of the circumferential velocity $|Wm|$ in some initial section of the wake to the corresponding value of the velocity deficit $|U_1^0|$ on the axis of the wake: $s = |Wm|/|U_1^0|$. For $|W_m| \cong |U_1^0| << U_\infty$ the swirl parameter $s_1 \cong 1$ and the swirling can be considered to be weak. If $|Wm| - U_\infty$ in the immediate vicinity of the rear of the body, such swirling should be considered to be strong. In this case $s_1 >> 1$. The above definition of the degree of swirl is fairly graphic, but does have the disadvantage that it may change, depending on the distance from the body.

All of the experiments were carried out for an airspeed $U_\infty = 15.3$ m/sec, which corresponds to the Reynolds number $Re = U_\infty D/\nu = 2.6 \cdot 10^4$ (ν is the kinematic viscosity), and five regimes of the nozzle that produces the compensating jet. The regimes can be changed by changing the airflow rate through the nozzle. The excess momentum and the angular momentum were varied at the same time. The quantitative changes of the experimental characteristics of the degree of swirling s and s_1, the degree of compensation of the drag of the body by the propeller thrust $\beta_x = J/F_x$ (F_x is the drag of the body without the propeller), as well as the dimensionless values of the excess momentum $J' = J/2\pi\rho U^2{}_\infty D^2$ and the angular momentum $M' = M/2\pi\rho U^2{}_\infty D^3$ are given in Table 1.

A point in the parameter plane $J'-M'$ corresponds to each of the regimes studied. For regimes 1 and 2 the propeller thrust was insufficient to balance the drag of the body and so $J' < 0$, $\beta < 0$. A momentumless wake ($J' = 0$, $\beta = 0$) with a nonzero integrated swirl developed behind the body in regime 3. In regimes 4 and 5 the propeller thrust exceeded the drag of the body and so $J' > 0$, $\beta > 0$. The momentum and angular momentum were estimated from the measured distribution $U_1(r)$ and $W(r)$ from Eqs. (2.1) and (2.2), in which the contribution of the terms due the velocity fluctuations was small. The values of s_1 were determined by using the data obtained in the wake section $\zeta = 7$.

3. The results of the measurements of $U_* = U_1/U_\infty$ and $W_* = W/U_\infty$ are shown in Figs. 2 and 3 as functions of $\xi = r/D$. The right side of these figures as well as in Fig. 4 show the data measured in the plane $\varphi = 0$ and the left side, in the plane $\varphi = \pi$. Curves *a-d* in Figs. 2-4 represent the results obtained at relative distances $\zeta = 7$, 10, 20, 50, respectively, from the body and the points represent regimes 1, 3, 5 of the nozzle. All three components of the velocity vector were measured in the experiments, but one of them (radial) was small. The angle β was also small.

In the wakes behind self-propelled bodies $U_*(\xi)$ profiles are formed as a result of the interaction of perturbations caused in the flow by the streamlined body and the propeller. In momentumless wakes without a swirl, which were studied , e.g., in [1, 5], the distribution of U_* in the paraxial region was determined by the jet flow produced by the propeller. The flow velocity here exceeded U_∞ and $U^0{}_* > 0$ ($U^0{}_*$ is the value of U_* at the axis of the wake). In the annular peripheral zone of the wake $U_* < 0$. This strictly is the wake of the body. In the case under consideration the swirl created centrifugal forces, which redistributed the total momentum so that the jet region with $J > 0$, $U_* > 0$ became peripheral and an interior with $J < 0$, $U_* < 0$ was formed in the wake behind the body with a propeller [3]. An initial profile of $U_*(\xi)$, which differs fundamentally from that in [1, 5], therefore, can be formed by means of a swirl in the wake behind a self-propelled body. Together with the slight deviations of the integrated momentum from zero the shape of the initial profile of U_* to a considerable extent determines the further evolution of the wake.

For $J > 0$ or $J < 0$, as the distance from the body increases the $U_*(\xi)$ profile is transformed so that sooner or later it takes on a shape that is typical of either a jet in the wake flow or a wake behind a towed body, respectively. Clearly, the distance ζ at which such a changeover of the flow occurs depends on the excess momentum and on the shape of the initial distribution of U_*. While $U_* < 0$ in the paraxial region of the wake for $J < 0$, the flow become purely a "wake" flow even at a short distance from the body, this distance being shorter when the difference of J from zero is greater. For $J < 0$ and $U^0{}_* > 0$ the changeover of the flow should take longer since initially the positive velocity deficit at the axis is transformed into a negative deficit, passing through the value $U^0{}_* = 0$. A different transformation of the $U_*(\xi)$ profile should be expected for $J > 0$. If the initial distribution of the deficit is such that $U^0{}_* > 0$, a purely jet flow is established fairly quickly and conversely, if $U^0{}_* < 0$, then as ζ increases $U^0{}_*$ changes sign and the transformation of the flow is prolonged.

It turned out that $U^0{}_* < 0$ for all propeller modes in the experiments conducted. Consequently, for $J < 0$ in regime 1 even when $\zeta \geq 20$ the U_* profile does not have a region with $U_* > 0$ and the profile itself resembles a typical velocity deficit distribution in the wake behind a towed body. In regime 5 we have $J > 0$ and the U_* profile at the distances studied

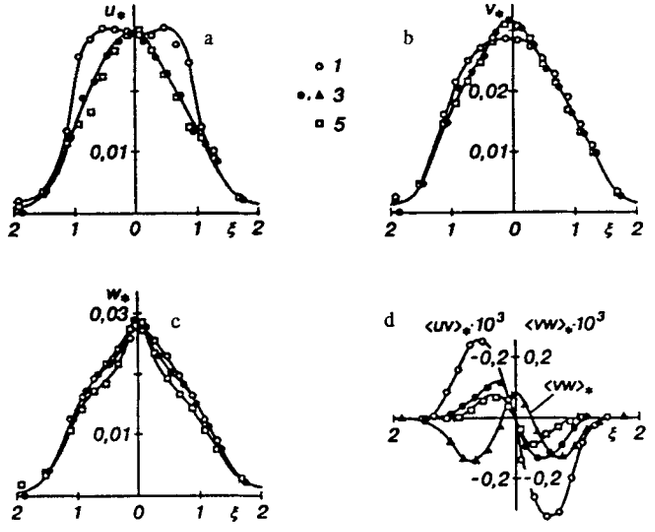

Fig. 4

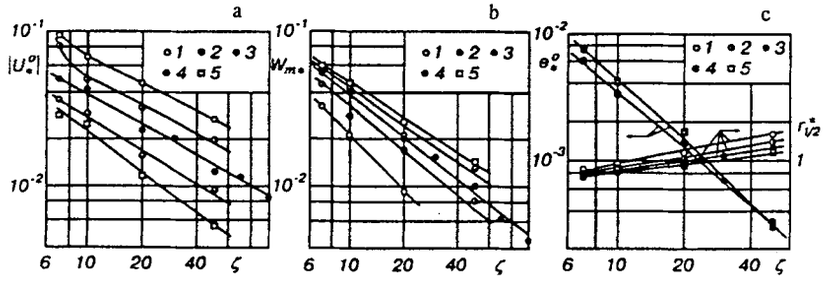

Fig. 5

continues to be of alternating sign and does not attain the shape characteristic of a jet flow. An increase in the ratio of the maximum U_*, taken from the jet part of the profile, to $|U_*^0|$ can, for example, be evidence of such a changeover. For regime 5 that ratio is 0.31 for $\zeta = 7$, 0.52 for $\zeta = 20$, and 0.63 for $\zeta = 50$.

If the mean velocity deficit in the swirling wake behind a sphere differs substantially in shape from the distribution of the longitudinal velocity component in the swirling jet, the change in the circumferential velocity $W_*(\xi)$ (see Fig. 3) in those flows is qualitatively similar in nature and resembles the velocity field of a single vortex core with a rectilinear axis, which coincides with the wake axis. In the immediate vicinity of the wake axis $W_* \sim \xi$, i.e., the liquid rotates like a solid in this region. As the swirling increases the region becomes smaller and the maximum circumferential velocity in a given section of the wake W_{m*} increases monotonically. The profiles in Fig. 3*d* do not include the profile of the circumferential velocity for a series of experiments with the smallest degree of swirling in the flow (regime 1). As will be demonstrated below, the velocity perturbations due to rotation degenerate rather rapidly in this case and W for $\zeta = 50$ was so small that it could not be recorded reliably.

Figure 4*a-d* shows typical transverse distributions of the intensities of the longitudinal $u_* = \langle u^2\rangle^{1/2}/U_\infty$, transverse $v_* = \langle v^2\rangle^{1/2}/U_\infty$, and tangential $w_* = \langle w^2\rangle^{1/2}/U_\infty$ components of the pulsation component of the velocity, as well as the correlations $\langle uv\rangle_* = \langle uv\rangle/U_\infty^2$, and $\langle vw\rangle_* = \langle vw\rangle/U_\infty^2$. These data pertain to the wake section $\zeta = 20$. The correlation $\langle uw\rangle$ was negligible in all the experiments.

Variation of the excess momentum and the angular momentum introduces important features during the formation and development of the turbulence field in the wake behind a sphere. Insufficient propeller thrust in comparison with the drag of the body and little swirling (regime 1) give rise to a turbulence, which even at short distances from the sphere acquires features that are characteristic of the wake behind a towed body. This appears most clearly in the transformation of the u_x profiles. For

small ζ the profiles are bell-shaped, but even for $\zeta \geq 20$ they become double-humped, similar to the corresponding u_* in wakes behind axisymmetric bodies without a propeller.

The distributions of two other components of the fluctuations v_* and w_* have a unimodal form as the swirling and propeller thrust and the u_* profile grow. The higher level of fluctuations in the paraxial zone of the wake is undoubtedly determined by the work of the propeller, as is manifested particularly clearly in the shape of the w_* profile, measured in regime 5. The behavior of the turbulence in this region most likely is not universal in the sense that the distribution of these characteristics are different in the wake swirled by another propeller (e.g., a screw).

As a result of the rapid degeneracy of the perturbations of the mean velocity field in a momentumless nonswirling wake the turbulence becomes almost shearless even at short distances from the body [1, 5]. A different picture is observed in a swirling wake, where not only the correlation $\langle uv \rangle$ but also the components of the velocity of the $\langle vw \rangle$ correlation are significant in the entire region of the flow (Fig. 4*d*). As can be seen, the $\langle uv \rangle_*$ profile is such that points where $\langle uv \rangle_* = 0$ roughly coincide with points where $\partial U_1 / \partial r = 0$. This is evidence that the gradient hypothesis $-\langle uv \rangle = \nu_T \partial U_1 / \partial r$, where ν_T is the viscosity coefficient.

Similar relations for the correlation $\langle vw \rangle$ should have the form $-\langle vw \rangle = \nu_T r \partial / \partial r (W/r)$. In the paraxial region of a momentumless swirling wake (regime 3), however, this equality with a finite value of ν_T does not obtain since $W(r) \sim r$ and $\partial / \partial r (W/r) = 0$ for small values of r, while $\langle vw \rangle \neq 0$.

The variations of J and M affect the transverse distributions of some characteristics of the turbulence as well as the distinctive features of the degeneracy in the wake. This is illustrated by Fig. 5*a-c*, which gives data on the behavior of U^0_* W_{m*}, e^0_*, and $r^*_{1/2}$ as a function of ζ (e^0_* is the energy of turbulence at the wake axis, $r^*_{1/2} = r_{1/2}/D$ is the characteristic transverse dimension of the wake as determined from the condition $u_*{}^0(r_{1/2}) = 0.5\, u^0_*$, and u^0_* is the intensity of the fluctuations of the longitudinal velocity component for $r = 0$); the points represent regimes 1-5.

In the series of experiments conducted a self-similar flow regime is possible in the wake for $J = 0$, while for $J < 0$ or $J > 0$ the flow may change over to a purely "wake" flow or a purely "jet" flow at the given distances from the body. For $J < 0$ (regimes 1, 2) and $\zeta > 10$ the change in $U^0_*(\zeta)$ is practically proportional to $\zeta^{-2/3}$, which is characteristic of a self-similar wake behind a towed body. Lower values and rather rapid degeneration of W_{m*} correspond to this series of experiments.

The decrease in U^0_* is most rapid for $J > 0$ (regimes 4, 5). Such development of the wake is due to the need for the initial distribution $U_*(\zeta)$ with $U^0_* < 0$ to change over to a form that is typical of jet flow with $U^0_* > 0$. In this series of experiments the values of W_{m*} are maximum and the degeneration of the circumferential component of the velocity is the slowest.

The existence of weak swirling of the flow in a momentumless wake ($J = 0$, regime 3) has a strong influence on the rate at which the deficit of the axial velocity component dies out in comparison with the case of wake that is also momentumless but does not swirl. While $U^0_* \sim \zeta^{-1.9}$ was obtained in [1] for $J = 0$, $M = 0$, the experiments performed gave $U^0_* \sim \zeta^{-0.7}$ for $J = 0$, $M \neq 0$. The rotational velocity component decreases somewhat more rapidly in this propeller regime so that the influence of the swirling should become weaker as ζ increases. No appreciable manifestation of this process has been detected, however, at the studied distances.

In contrast to the appreciable effect of variations of the excess momentum and angular momentum on the degeneracy of the mean velocity field, the decay of the turbulent energy $e_* = (u_*^2 + v_*^2 + w_*^2)/2$, shown in Fig. 5*c*, is almost independent of those variations. Moreover, the slight difference between the values of e^0_* for small ζ for regimes 1 and 2 from the values of e^0_* for regimes 3-5 decreases with increasing ζ. At the same time, the swirl of the flow in the wake causes slower degeneration of the turbulent energy in a momentumless wake $e^0_* \sim \zeta^{-1.5}$, while $e^0_* \sim \zeta^{-1.9}$ was obtained for $J = 0$, $M = 0$ in [1].

The data on $r^*_{1/2}(\zeta)$, also shown in Fig. 5, give a graphic idea of the growth of the characteristic transverse dimensions of the given wake downstream. While $r^*_{1/2}$ in regime 1 increases roughly the same way as in a wake behind a body without a propeller, i.e., $\sim \zeta^{1/3}$, as the degree of swirl rises the increase in the transverse dimensions of the wake slows down monotonically in regime 5, i.e., $r^*_{1/2} \sim \zeta^{0.18}$. The thickness of a swirling momentumless wake also increases more slowly ($r^*_{1/2} \sim \zeta^{0.24}$) in comparison with the dimensions of the wake without swirling ($r^*_{1/2} \sim \zeta^{0.43}$) (see [1]).

We thank V. I. Bukreev for useful discussions of the work and E. M. Romanov for assistance in preparing and conducting the experiments.

REFERENCES

1. N. V. Aleksenko and V. A. Kostomakha, "Experimental study of an axisymmetric momentumless turbulent jet flow," Prikl. Mekh. Tekh. Fiz., No. 1 (1971).
2. A. S. Ginevskii, Theory of Turbulent Jets and Wakes [in Russian], Mashinostroenie, Moscow (1969).
3. J. A. Shetz and A. K. Jakubowski, "Experimental studies of the turbulent wake behind self-propelled slender body," AIAA J., **13**, No. 12 (1975).
4. L. N. Voitovich, "Experimental studies of turbulent jet flows," in: Industrial Aerodynamics/Aerodynamics of Rotodynamic Machines, Channels, and Jet Flows [in Russian], Mashinostroenie, Moscow (1968).
5. E. Naudascher, "Flow in the wake of self-propelled body and related sources of turbulence," J. Fluid Mech., **22**, No. 4 (1965).
6. V. A. Kostomakha and N. V. Lesnova, "Turbulent axisymmetric momentumless wake in turbulized and non-turbulized external flow," Proc. Bulgarian Ship Hydrodynamics Centre, **1** (1989).
7. H. Higuchi and T. Kubota, "Axisymmetric wakes behind a slender body including zero-momentum configuration," Phys. Fluids., **2**, No. 9 (1990).
8. G. Birkoff and E. Sarantello, Jets, Wakes, and Caverns [Russian translation], Mir, Moscow (1964).
9. V. A. Gorodtsov, "Self-similarity and weak closing relations symmetric free turbulence," Izv. Akad. Nauk SSSR, Mekh. Zhidk. Gaza, No. 1 (1979).
10. V. A. Sabel'nikov, "Some distinctive features of turbulent flows with zero excess momentum," Uch. Zap., TsAGI, **6**, No. 3 (1975).
11. M. L. Finson, "Similarity behavior of momentumless turbulent wakes," J. Fluid. Mech. **71**, No. 3 (1975).
12. A. I. Korneev, "Similarity hypotheses in the theory of turbulent jet flows," in: Turbulent Flows [in Russian], Nauka, Moscow (1977).
13. S. Hassid, "Similarity and decay laws of momentumless wakes," Phys. Fluids, **23**., No. 2 (1980).
14. B. A. Kolovandin and N. N. Luchko, "Numerical simulation of the velocity of an axisymmetric momentumless wake," in: Proc. of Conference on Heat and Mass Transfer. Teplomassoobmen-VI [in Russian], Part 2 (1980).
15. N. N. Fedorova and G. G. Chernykh, "Numerical simulation of a momentumless turbulent wake behind a sphere," Modelirovanie Mekh., **6** , No. 1, ITPM. Sib. Otd. Ross. Akad. Nauk, Novosibirsk (1992).
16. A. Reynolds, "Similarity in swirling wakes and jets," J. Fluid. Mech., **15**, No. 2 (1962).
17. A. G. Gumilevskii, "Study of momentumless swirling wakes on the basis of a two-parameter model of turbulence," Izv. Ross. Akad. Nauk. Mekh. Zhidk. Gaza, No. 3 (1992).
18. A. G. Gumilevskii, "Violation of self-similarity in turbulent axisymmetric swirling wakes," Izv. Ross. Akad. Nauk. Mekh. Zhidk. Gaza, No. 1 (1993).
19. A. G. Gumilevskii, "Self-similarity and laws of degeneracy in wakes with compensation for momentum and angular momentum," Izv. Ross. Akad. Nauk. Mekh. Zhidk. Gaza, No. 5 (1993).
20. H. Fujita and L. S. G. Kovasnai, "Reynolds stress measurements using a hot-wire anemometer with a single rotating filament," Prib. Nauch. Issled., **39**, No. 9 (1968).
21. G. E. Sturov, "Method of hot-wire anemometer measurement in three-dimensional turbulent flows," Dinamika Sploshn. Sredy, Inst. Gidrodinamiki, Sib. Otd., Akad. Nauk SSSR, No. 8 (1971).
22. J. O. Hinze, Turbulence, 2nd. ed., McGraw-Hill, New York (1975).
23. P. Bradshaw, An Introduction to Turbulence and Its Measurements, Pergamon, Oxford (1975).
24. L. W. B. Browne, R. A. Antonia, and L. P. Chua, "Calibration of X-probes for turbulent flow measurements," Exp. Fluids, **7**, No. 3 (1989).